8th ECCOMAS Thematic Conference on the Mechanical Response of Composites
COMPOSITES 2021
M. Fagerström & C. Catalanotti (Editors)

INVESTIGATION OF POWER CONTRIBUTIONS OF REPEATING UNIT CELLS OF CARBON FIBER REINFORCED PLASTICS AT FAILURE

Lukas M. Poggenpohl, Jaan W. Simon

Institute of Applied Mechanics, RWTH Aachen University,
Mies-van-der-Rohe-Str. 1, 52074 Aachen, Germany

Keywords: Material Modeling, Nonlocal, Damage.

Summary: *Carbon fiber reinforced plastics are used in many applications. In recent publications, repeating unit cells (RUCs) undergoing localization phenomena are investigated and homogenized. In this paper, aspects of the homogenization approaches are investigated analytically and numerically.*

1. INTRODUCTION

The use of carbon fiber reinforced plastics (CFRPs) has increased over the past decades. Due to their high specific strength and stiffness, the use of CFRPs and composite materials in aerospace applications has increased trougout the years (see, e.g.[1]). Their high specific stiffness and high specific strength make CFRPs an ideal material for light weight construction (see, e.g.[2]).

CFRPs generally fail in a brittle manner (see, e.g. [3]). Therefore, high safety factors have to be applied in the design phase of structures made of CFRPs. This remedy, together with the high manufacturing costs, is assumed to be one of the main draw backs preventing a wide range use of CFRPs as material of construction.

The micro and meso scale analysis using repeating unit cells (RUCs) has proven to give a good insight into the phenomenon at the microscale and how they influence the macroscopic response of the material. For instance, in a recent publication [4], an analysis of the elastic and plastic response of CFRPs is given, where RUCs are used for homogenization at the fiber level (micro scale) and the yarn level (meso scale). The numerical results are compared to experimental data and show a good agreement. However, standard Hill's approach ([5, 6]) is used here for homogenization of the RUCs and a size convergence study is applied only for the elastic response.

As shown in several publications (e.g. [7, 8, 9]), standard Hill's approach breaks down at the presence of strain softening as it is induced by damage and failure. As shown in [8], it is not possible to determine a representative RUC size using Hill's approach. It is concluded in said publication that this remedy is caused by a mismatch of sizes of the localization band (i.e. dissipative volume) and the overall size of the RUC (i.e. elastic energy volume), since the ratio of dissipative volume and elastic energy volume is not constant but scales with $1/L$ of a typical length scale of the RUC.

As shown in [10], a representative RUC size can be found when applying the so called failure zone averaging. A similar approach is used in [11, 12] for cracks within the RUC. However, in [10] and following publications [13, 14, 15] only numerical evidence for the accuracy of the failure zone averaging is shown.

In this paper, simulations of one exemplary RUC with a brittle damaging material model for the epoxy matrix will be shown and the numerical evidence of [10] will be analyzed numerically by means of a parameter study.

2. Material model

The material model used in this publication is based on the isotropic part of the material model presented in [16]. In the following, the important aspects will be given, whereas the details of implementation can be found in this publication.

2.1 Helmholz free energy

The material model used is a St. Venant-Kirchhoff type material model involving a brittle damage function:

$$\psi_{mech}(\boldsymbol{E}, D) = (1-D)^n \psi_e(\boldsymbol{E}) = (1-D)^n \left(\frac{E}{2} \operatorname{tr}[\boldsymbol{E}]^2 + \mu \operatorname{tr}[\boldsymbol{E}^2] \right) \tag{1}$$

In equation 1, E is the Youngs' Modulus and μ is the shear modulus. Variable D is the so called local damage variable ranging from 0 (i.e. virgin material) to 1 (i.e. broken material, complete loss of stresses and stiffness) and $\boldsymbol{E}$ is the Green-Lagrange strain tensor defined as

$$\boldsymbol{E} = \frac{1}{2}(\boldsymbol{F}^T \boldsymbol{F} - \boldsymbol{I}) \tag{2}$$

with $\boldsymbol{F}$ being the deformation gradient. Variable n is the damage exponent and generally is given as a positive integer value. The most common choices are $n = 1$ for a strain equivalent model and $n = 2$ for an energy equivalent model. The mechanical energy is then enhanced with a damage hardening term (ψ_h) and two micromorphic terms (ψ_g and ψ_χ) as introduced in [17, 18, 19]:

$$\psi(\boldsymbol{E}, D) = \psi_{mech}(\boldsymbol{E}, D) + \psi_h(D) + \psi_g(\nabla_0 D^\chi) + \psi_\chi(D, D^\chi) \tag{3}$$

Here, D^χ is the so called micromorphic damage variable which is introduced as an additional degree of freedom and ∇_0 is the spacial gradient with respect to the reference configuration. A linear damage hardening function is chosen. Therefore, ψ_h reads

$$\psi_h = \frac{K}{2} D^2 \tag{4}$$

with K being a material parameter of choice.

The micromorphic energies read

$$\psi_\chi = \frac{H^\chi}{2}\left(D^\chi - D\right)^2 \quad \text{and} \tag{5}$$

$$\psi_g = \frac{El^2}{2}\left(\nabla_0 D^\chi \cdot \nabla_0 D^\chi\right), \tag{6}$$

respectively. As can be seen from Eq. (5), ψ_χ is a penalty energy which couples the local damage variable D and its micromorphic counterpart D^χ. Parameter H^χ regulates the difference between D and D^χ and is generally chosen quite large. Term ψ_g in Eq. (6) is the so called gradient term and penalizes high gradients of D^χ. As in [20], the length scale parameter l is introduced and scaled with the Youngs' modulus. This yields the advantage of having a length like variable control the width of the failure zone.

2.2 Clausius-Duhem inequality

Inserting the given free energy terms into the Clausius-Duhem inequality yields an extended version of the dissipation inequality.

$$-\dot{\psi} + \boldsymbol{S} \cdot \dot{\boldsymbol{E}} + \underbrace{a\dot{D}^\chi + \boldsymbol{b} \cdot \nabla_0 \dot{D}^\chi}_{\text{micromorphic extension}} \geq 0 \tag{7}$$

Here, the stress like counter parts a and $\boldsymbol{b}$ of the micromorphic damage variable (D^χ) and its gradient ($\nabla_0 D^\chi$) are given, respectively. Application of the chain rule to the free energy term yields:

$$\left(\boldsymbol{S} - \frac{\partial \psi}{\partial \boldsymbol{E}}\right) \cdot \dot{\boldsymbol{E}} + \left(a - \frac{\partial \psi}{\partial D^\chi}\right) \dot{D}^\chi + \left(\boldsymbol{b} - \frac{\partial \psi}{\partial \nabla_0 D^\chi}\right) \cdot \nabla_0 \dot{D}^\chi - \frac{\partial \psi}{\partial D}\dot{D} \geq 0 \tag{8}$$

To ensure this inequality holds for arbitrary processes the braces are individually chosen to be equal to zero, which yields the following relations:

$$\boldsymbol{S} = \frac{\partial \psi}{\partial \boldsymbol{E}}, \quad a = \frac{\partial \psi}{\partial D^\chi}, \quad \boldsymbol{b} = \frac{\partial \psi}{\partial \nabla_0 D^\chi} \tag{9}$$

The remaining dissipation inequality

$$\underbrace{-\frac{\partial \psi}{\partial D}}_{=:Y}\dot{D} \geq 0 \tag{10}$$

has to be solved. Here, Y indicates the damage driving force, which for the material model presented reads

$$Y = n(1-D)^{n-1}\psi_e + H^\chi\left(D^\chi - D\right) - KD. \tag{11}$$

From Eq. (11), the coupling of the local and micromorphic damage variable becomes apparent. If D^χ is lower than D, the damage driving force is reduced, whereas for D^χ larger than D it is increased. The remaining dissipation inequality is then fulfilled using a loading function

$$\Phi(Y) = Y - Y_0 \tag{12}$$

as well as loading and unloading conditions (see, e.g. [21]). Parameter Y_0 in Eq. (12) is the so called damage threshold comparable to the yield strength in plasticity. For the given damage model the loading and unloading conditions, which are comparable to the Karush-Kuhn-Tucker conditions, read:

$$\dot{D} \geq 0, \quad \dot{D}\Phi = 0, \quad \Phi \leq 0 \tag{13}$$

2.3 Boundary value problem

As described earlier, the micromorphic damage variable D^χ is introduced as an additional degree of freedom. Thus, an additional balace equation, the micromorphic balance equation, has to be solved additionally to balance of linear momentum. The whole set of balance equations read:

$$\mathrm{Div}\,(\boldsymbol{F}\boldsymbol{S}) + \boldsymbol{f}_0 = \boldsymbol{0}\,; \quad \mathrm{Div}\,(\boldsymbol{b}) - a = 0 \quad \text{in} \quad \Omega_0 \tag{14}$$

Here, Ω_0 describes the computational domain (i.e. the simulated body) at the reference configuration and $\boldsymbol{f}_0$ is the body force acting on the material point in the reference configuration. The second balance equation can be expanded by applying Eq. (9) as well as Eqs. (5) and (4) and then reads:

$$0 = H^\chi(D^\chi - D) - El^2\nabla_0\left(\nabla_0 D^\chi\right) \quad \text{in} \quad \Omega_0 \tag{15}$$

As schown e.g. in [22] and [23], boundary conditions have to be applied to the mechanical part as well as to the micromorphic part. Here, these boundary conditions read:

$$\begin{aligned} &\underline{\text{BC for balance of linear momentum:}} && \underline{\text{BC for micromorphic balance:}} \\ &(\boldsymbol{F}\boldsymbol{S})\boldsymbol{n}_0 = \hat{\boldsymbol{t}}_0 \quad \text{on} \quad \partial\Omega_{0,n} && \nabla_0 D^\chi \cdot \boldsymbol{n}_0 = 0 \quad \text{on} \quad \partial\Omega_0 \\ &\boldsymbol{u} = \hat{\boldsymbol{u}} \quad \text{on} \quad \partial\Omega_{0,d} \end{aligned} \tag{16}$$

In Eqs. (16), $\hat{\boldsymbol{t}}_0$ and $\hat{\boldsymbol{u}}$ are the prescribed tractions and displacements at the boundary of the undeformed body Ω_0. From Eq. (16), the Neumann ($\partial\Omega_{0,n}$) and a Dirichlet ($\partial\Omega_{0,d}$) boundary conditions for the balance of linear momentum become apparent. In case of the micromorphic balance equation, only Neumann type boundary conditions are prescribed on $\partial\Omega_0$.

3. Power contributions

As referenced in Sec. 1, in [14] numerical evidence is given, that the Hill condition holds for the failure zone averaging technique introduced in [10]. However, as seen in the previous section, a micromorphic extension also contributes to the total energy. As shown in [23], the

micromorphic virtual work vanishes when averaging over the whole body. In the following, a derivation for the given material model following the steps in [23] will be shown.

Let us consider an RUC with the computational domain Ω_0. The Hill condition states, that the virtual macroscopic work and the averaged virtual microscopic work are equal:

$$\{\boldsymbol{S}\}_{\Omega_0} \cdot \{\delta \boldsymbol{E}\}_{\Omega_0} = \frac{1}{|\Omega_0|} \int_{\Omega_0} (\boldsymbol{S} \cdot \delta \boldsymbol{E} + a\, \delta D^\chi + \boldsymbol{b} \cdot \delta \nabla_0 D^\chi)\, \mathrm{dV} \tag{17}$$

Here, $\{*\}_{\Omega_0}$ denotes the volume average of a given quantity, i.e.:

$$\{*\}_{\Omega_0} = \frac{1}{|\Omega_0|} \int_{\Omega_0} * \, \mathrm{dV} \tag{18}$$

Application of the product rule to the last term of Eq. (17) yields:

$$\begin{aligned} & \mathrm{Div}(\boldsymbol{b} \cdot \delta D^\chi) = \mathrm{Div}(\boldsymbol{b}) \delta D^\chi + \boldsymbol{b} \cdot \nabla_0 D^\chi \\ \Leftrightarrow \quad & \boldsymbol{b} \cdot \delta \nabla_0 D^\chi = \mathrm{Div}(\boldsymbol{b} \cdot \delta D^\chi) - \mathrm{Div}(\boldsymbol{b}) \delta D^\chi \end{aligned} \tag{19}$$

The balance equation of the micromorphic extension (14) can be rewritten to get:

$$\mathrm{Div}(\boldsymbol{b}) = a \tag{20}$$

As shown in Eq. (16), the gradient of D^χ has to vanish at the boundary. Having this in mind and applying (9) to (16), a boundary condition for $\boldsymbol{b}$ can be derived:

$$\boldsymbol{b} \cdot \boldsymbol{n}_0 = El^2\, \nabla_0 D^\chi \cdot \boldsymbol{n}_0 = 0 \quad \text{on } \partial\Omega_0 \tag{21}$$

Application of Eqs. (19) to (21) to the virtual work of the micromorphic extension leads to:

$$\int_{\Omega_0} (a\, \delta D^\chi + \boldsymbol{b} \cdot \delta \nabla_0 D^\chi) \mathrm{dV} \tag{22}$$

$$\Leftrightarrow \quad \int_{\Omega_0} (a\, \delta D^\chi + \mathrm{Div}(\boldsymbol{b} \cdot \delta D^\chi) - a\, \delta D^\chi) \mathrm{dV} \tag{23}$$

$$\Leftrightarrow \quad \int_{\Omega_0} \mathrm{Div}(\boldsymbol{b} \cdot \delta D^\chi) \mathrm{dV} = \int_{\partial\Omega_0} \boldsymbol{b} \cdot \boldsymbol{n}_0\, \delta D^\chi \mathrm{dA} = 0 \tag{24}$$

From Eq. (24) it becomes apparent that the micromorphic energy has to vanish if integrated over the whole volume of a the computed body. However it is questionable, whether this holds true, if the failure zone averaging is applied and the integrated volume changes from Ω_0 to Ω_d with

$$\Omega_d = \{\boldsymbol{x}\, \epsilon\, \Omega_0 \mid \dot{D}(\boldsymbol{x}) > 0\}. \tag{25}$$

In the following, this question is addressed by means of numerical results. For this, the mechanical ($\mathcal{P}_{mech}$) and micromorphic powers ($\mathcal{P}_{\chi}$ or $\mathcal{P}_{\chi,d}$) are defined as follows:

$$\mathcal{P}_{mech} = \int_{\Omega_0} (\boldsymbol{S} \cdot \Delta \boldsymbol{E}) \, \mathrm{dV} \tag{26}$$

$$\mathcal{P}_{\chi} = \int_{\Omega_0} (a \, \Delta D^{\chi} + \boldsymbol{b} \cdot \Delta \nabla_0 D^{\chi}) \, \mathrm{dV} \tag{27}$$

$$\mathcal{P}_{\chi,d} = \int_{\Omega_d} (a \, \Delta D^{\chi} + \boldsymbol{b} \cdot \Delta \nabla_0 D^{\chi}) \, \mathrm{dV} \tag{28}$$

In above equations, Δ denotes the numerical differential with respect to the given time step (i.e. $\Delta(*) = d*/dt$). For this, the micromorphic power is either integrated over the whole domain or over the actively damaging domain giving $\mathcal{P}_{\chi}$ or $\mathcal{P}_{\chi,d}$, respectively.

4. Numerical results

The material model introduced in Section 2 is implemented in the finite element software FEAP by means of a user material and a user element. The material simulated is long fiber reinforced plastic, where the fibers were assumed to be linear elastic. It shall be mentioned that a pseudo viscosity term (as shown e.g. in [20]) was introduced to prevent snapback behavior. The fibers were simulated as perfect cylinders with a diameter of $7\,\mu\mathrm{m}$ and were placed in a regular grid into an RUC of size $60\,\mu\mathrm{m} \times 60\,\mu\mathrm{m} \times 1\,\mu\mathrm{m}$. In total, 50 fibers were used which results in a fiber fraction of approximately 54%. Periodic boundary conditions were applied and the RUC is subjected to a far field strain of up to 5% in x-direction. The geometry is visualized in Fig. 1.

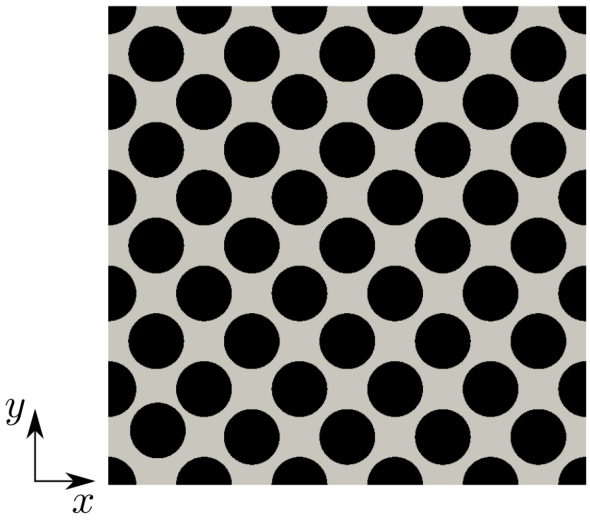

Figure 1. Geometry used for RUC simulation; grey: resin matrix, black: carbon fibers

The material parameters used for fiber and matrix are summarized in Tab. 1. The mechanical parameters were taken from [16]. Index 1 denotes material parameters which were associated with the matrix material, while index 2 denotes material parameters which were associated with the fibers. If no index is set, the material parameters were the same for fiber and matrix. The micromorphic length l_1 was chosen in a way, that a sufficiently large localization band was formed. Pseudo viscosity η was chosen to be as small as possible while still achieving numerical stability. The yield strength of the fibers was chosen numerical infinity (i.e. $Y_2 = 10 \times 10^8\,\mathrm{MPa}$) and the micromorphic parameters of the fibers were chosen in a way that they did not interact with the micromorphic field.

Table 1. Material parameters for the resin matrix (index 1) and carbon fibers (index 2).

Parameter	Value	Parameter	value	Parameter	value
λ_1	$5308\,\mathrm{MPa}$	μ_1	$3538\,\mathrm{MPa}$	Y_1	$0.0672\,\mathrm{MPa}$
l_1	$1.95 \times 10^{-2}\mathrm{mm}$	K_1	$0.205\,\mathrm{MPa}$	n_1	2
H_1^χ	$2 \times 10^4\mathrm{MPa}$				
η	$1 \times 10^{-3}\,\mathrm{MPa}$				
λ_2	$423\,077\,\mathrm{MPa}$	μ_2	$84\,615\,\mathrm{MPa}$	Y_2	$10 \times 10^8\,\mathrm{MPa}$
H_2^χ	$1\,\mathrm{MPa}$	l_2	0.0		

In a mesh convergence study it was found, that a mesh size of $0.5\,\mu\mathrm{m}$ is sufficiently accurate. In the following the results of a parameter study are given, where the micromorphic parameters l_1 and H_1^χ were varied. For convenience, the prefactors α and β are introduced in this publication. The actual parameters for each of the simulations were $l_{comp} = \alpha \cdot l_1$ and $H_{comp}^\chi = \beta \cdot H_1^\chi$, respectively. The mechanical and micromorphic powers were computed for each gauss point and integrated over the RUC (i.e. Ω_0).

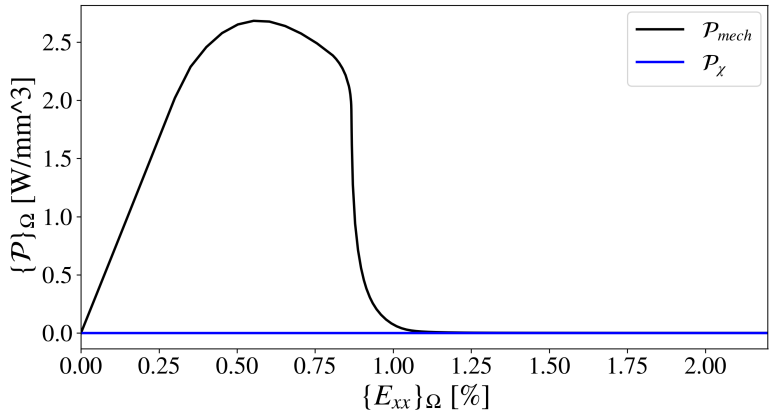

Figure 2. Mechanical and micromorphic power integrated over the whole computational domain; Parameters: $\alpha = 0.5$, $\beta = 0.02$

In Fig. 2 the mechanical and micromorphic powers are shown. It becomes evident that the micromorphic power is zero when it is integrated over the whole computational domain. This is in accordance with the theoretical results found in Sec. 3.

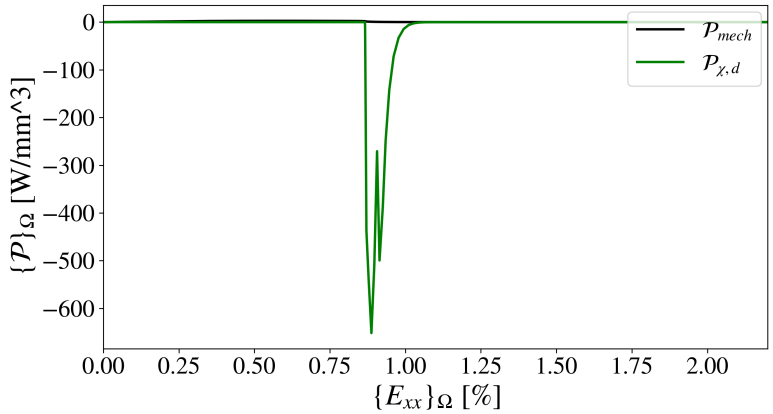

Figure 3. Mechanic power density of the computational domain Ω_0 and micromorphic power of the actively damaging domain Ω_d plotted with respect to the average strain; Parameters: $\alpha = 0.5$, $\beta = 0.02$

In Fig. 3, a comparison of the mechanical power ($\mathcal{P}_{mech}$) as shown in previous Fig. 2 and the micromorphic power ($\mathcal{P}_{\chi,d}$) of the actively damaging domain are given. It can easily be seen that the micromorphic power in its maximum exceeded the highest mechanical power by several amplitudes in the means of absolute values. It shall be mentioned, that $\mathcal{P}_{\chi,d}$ only is a part of the overall power contribution. Therefore, it can be negative without harming the second law of thermodynamics. Comparing Figs.3 and 2 it becomes apparent, that the micromorphic power was the highest, when final load drop occurred (i.e. the final failure and crack opening happened). This is strong evidence, that the micromorphic power contribution should be considered, if failure zone averaging is applied.

In Fig. 4, the results of the parameter study are summarized. Here, the quotient of the overall mechanical work ($\mathcal{W}_{mech}$) and micromorphic work of the actively damaging domain ($\mathcal{W}_{mic,d}$) was used for comparison. The work was defined as the time integral of the power ($\mathcal{W} = \int \mathcal{P}\ \mathrm{d}t$) and numerically integrated via the mid point rule.

As can be seen from the results in Fig. 4, the quotient showed a strong dependence on low values of parameter β where for high values, the results were almost the same. Lower constrains on differences between the local and nonlocal damage value lead to a higher quotient. In case of parameter α it can be seen that a value of 1 lead to the highest quotients where lower and higher values of α gave lower quotients. Overall, a parameter combination of low values for β and $\alpha = 1$ gave the highest quotients of micromorphic and mechanical work. Lower values for β were tested as well, but it was not possible to finish those computations.

From Figs. 4 it becomes apparent, that the overall micromorphic work was small compared to the overall mechanical work. This is in contradiction to the results given in Fig. 3, where

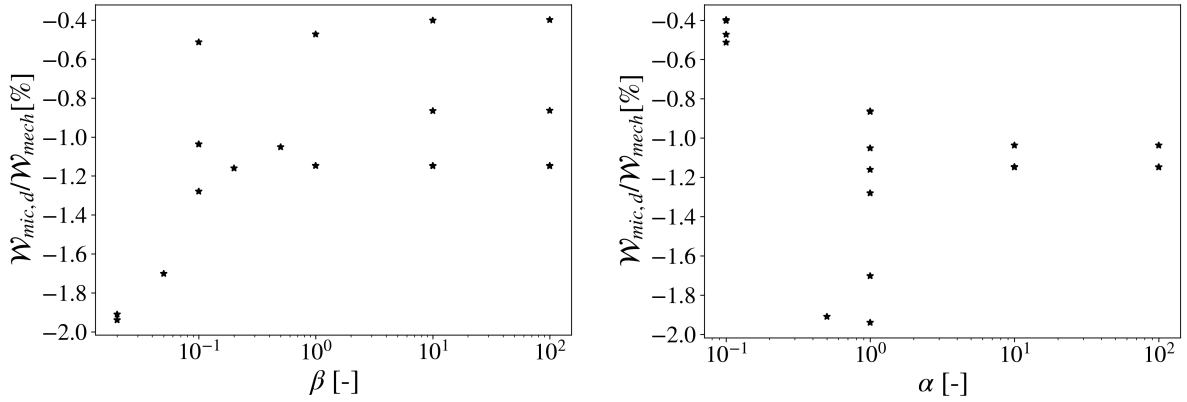

(a) c (b) c

Figure 4. Comparison of micromorphic work of the active damaging domain $\mathcal{W}_{mic,d}$ and overall mechanical work $\mathcal{W}_{mech}$ for different parameter combinations.

the micromorphic power was two magnitudes higher than the mechanical power. In Fig. 5, the same mechanical and micromorphic powers as in Fig. 3 are shown. Here, the powers were plotted with respect to the normalized computational time. It can be seen, that the micromorphic power showed significant values only for a short period of time when final failure occured, approximately $1 \times 10^{-4}\,\mathrm{s}$. Before and shortly after the peak, the micromorphic power tended to zero. If integrated over time, this short period of high power still is small.

5. Conclusion

In this publication, a parameter study of an RUC for long fiber reinforced plastics was performed. Aim of the study was to determine whether the micromorphic power and work can be neglected, when applying the failure zone averaging introduced in [10].

Following the derivations of [23] it was shown analytically that the micromorphic power should vanish when it is integrated over the whole computational domain. Numerical evidence supports this analytical derivation. However, strong evidence was found that the micromorphic power does not vanish if the failure zone averaging introduced in [10] is applied. Investigation of the mechanical and micromorphic powers showed that the latter one can be several magnitudes larger for a short amount of time. A parameter study for the micromorphic parameters l and H^{χ} was conducted and a parameter set for the highest quotient of micromorphic and mechanical work is found. Overall, the mechanical work was still larger than the micromorphic work. It was shown that the micromorphic power only shows high values for a short amount of time. Even though the peaks are high, this leads to small numerical values when itegrated over the whole computational time.

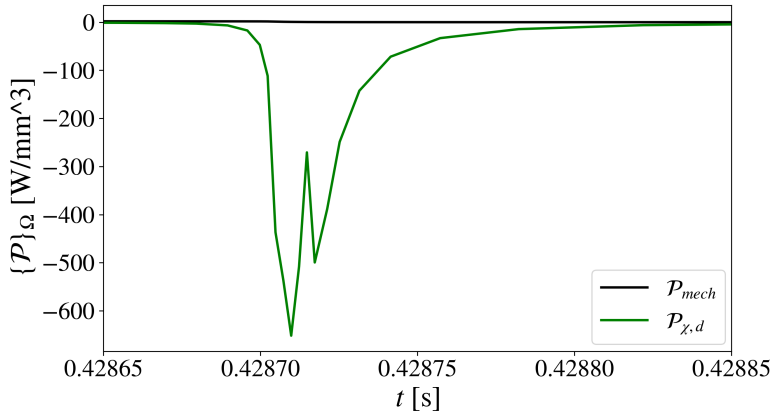

Figure 5. Mechanic power density of the computational domain Ω_0 and micromorphic power of the actively damaging domain Ω_d plottet with respect to the normalized computation time; Parameters: $\alpha = 0.5$, $\beta = 0.02$

Acknowledgements

The financial support of Deutsche Forschungsgemeinschaft (DFG, German Research Foundation) – project number: 423783552 – is gratefully acknowledged. Additionally, the authors would like to thank Prof. Dr. Stefanie Reese for her support.

References

[1] D. Ozkan, M. S. Gok, and A. C. Karaoglanli. *Carbon Fiber Reinforced Polymer (CFRP) Composite Materials, Their Characteristic Properties, Industrial Application Areas and Their Machinability*, pages 235–253. Springer International Publishing, Cham, 2020.

[2] J. Rösler, H. Hardes, and M. Bäcker. *Mechanisches Verhalten der Werkstoffe*. Springer-Verlag Berlin Heidelberg, 2013.

[3] K. Naresh, K. Shankar, R. Velmurugan, and N.K. Gupta. Statistical analysis of the tensile strength of gfrp, cfrp and hybrid composites. *Thin-Walled Structures*, 126:150–161, 2018. Special Issue on Plasticity and Impact Mechanics (IMPLAST 2016).

[4] C. He, J. Ge, B. Zhang, J. Gao, S. Zhong, W. K. Liu, and D. Fang. A hierarchical multiscale model for the elastic-plastic damage behavior of 3d braided composites at high temperature. *Composites Science and Technology*, 196:108230, 2020.

[5] R. Hill. The essential structure of constitutive laws for metal composites and polycrystals. *Journal of the Mechanics and Physics of Solids*, 15(2):79–95, 1967.

[6] R. Hill. On constitutive macro-variables for heterogeneous solids at finite strain. *Proceedings of the Royal Society of London. A. Mathematical and Physical Sciences*, 326(1565):131–147, 1972.

[7] I. M. Gitman, H. Askes, L. J. Sluys, and O. L. Valls. The concept of representative volume for elastic, hardening and softening materials. In *Proceedings of XXXII International Summer School-Conference 'Advance problems in Mechanics'*, pages 180–184, 2004.

[8] I.M. Gitman, H. Askes, and L.J. Sluys. Representative volume: Existence and size determination. *Engineering Fracture Mechanics*, 74(16):2518 – 2534, 2007.

[9] M.G.D. Geers, V.G. Kouznetsova, and W.A.M. Brekelmans. Multi-scale computational homogenization: Trends and challenges. *Journal of Computational and Applied Mathematics*, 234(7):2175 – 2182, 2010. Fourth International Conference on Advanced COmputational Methods in ENgineering (ACOMEN 2008).

[10] V. P. Nguyen, O. Lloberas-Valls, M. Stroeven, and L. J. Sluys. On the existence of representative volumes for softening quasi-brittle materials - a failure zone averaging scheme. *Computer Methods in Applied Mechanics and Engineering*, 199(45):3028 – 3038, 2010.

[11] S. Turteltaub, N. van Hoorn, W. Westbroek, and C. Hirsch. Multiscale analysis of mixed-mode fracture and effective traction-separation relations for composite materials. *Journal of the Mechanics and Physics of Solids*, 117:88 – 109, 2018.

[12] S. Turteltaub and G. de Jong. Multiscale modeling of the effect of sub-ply voids on the failure of composite materials. *International Journal of Solids and Structures*, 165:63 – 74, 2019.

[13] V. P. Nguyen, O. Lloberas-Valls, M. Stroeven, and L. J. Sluys. Computational homogenization for multiscale crack modeling. implementational and computational aspects. *International Journal for Numerical Methods in Engineering*, 89(2):192–226, 2012.

[14] V. P. Nguyen, O. Lloberas-Valls, M. Stroeven, and L. J. Sluys. Computational homogenization for multiscale crack modeling. implementational and computational aspects. *International Journal for Numerical Methods in Engineering*, 89(2):192–226, 2012.

[15] V. P. Nguyen, M. Stroeven, and L. J. Sluys. Multiscale failure modeling of concrete: Micromechanical modeling, discontinuous homogenization and parallel computations. *Computer Methods in Applied Mechanics and Engineering*, 201-204:139 – 156, 2012.

[16] L. Poggenpohl, T. Brepols, H. Holthusen, S. Wulfinghoff, and S. Reese. Towards brittle damage in carbon fiber reinforced plastics: A gradient extended approach. *Composite Structures*, page 112911, 2020.

[17] S. Forest. Micromorphic approach for gradient elasticity, viscoplasticity, and damage. *Journal of Engineering Mechanics*, 135(3):117–131, 2009.

[18] S. Forest. Nonlinear regularization operators as derived from the micromorphic approach to gradient elasticity, viscoplasticity and damage. *Proc. R. Soc. A*, 472(2188):20150755, 2016.

[19] T. Brepols, S. Wulfinghoff, and S. Reese. A gradient-extended two-surface damage-plasticity model for large deformations. *International Journal of Plasticity*, 129:102635, 2020.

[20] M. Fassin, R. Eggersmann, S. Wulfinghoff, and S. Reese. Efficient algorithmic incorporation of tension compression asymmetry into an anisotropic damage model. *Computer Methods in Applied Mechanics and Engineering*, 354:932 – 962, 2019.

[21] H. Holthusen, T. Brepols, S. Reese, and J.-W. Simon. An anisotropic constitutive model for fiber-reinforced materials including gradient-extended damage and plasticity at finite strains. *Theoretical and Applied Fracture Mechanics*, 108:102642, 2020.

[22] T. Brepols, S. Wulfinghoff, and S. Reese. Gradient-extended two-surface damage-plasticity: micromorphic formulation and numerical aspects. *International Journal of Plasticity*, 97:64–106, 2017.

[23] H. Clasen, C. B. Hirschberger, J. Korelc, and P. Wriggers. *Fe2-homogenization of micromorphic elasto-plastic materials*, page 280–291. CIMNE, 2013.